

# Structural relaxation in supercooled orthoterphenyl

S.-H. Chong\* and F. Sciortino

*Dipartimento di Fisica and Istituto Nazionale per la Fisica della Materia,  
Center for Statistical Mechanics and Complexity,  
Università di Roma “La Sapienza,” Piazzale Aldo Moro 2, I-00185, Roma, Italy  
(Dated: February 2, 2008)*

We report molecular-dynamics simulation results performed for a model of molecular liquid orthoterphenyl in supercooled states, which we then compare with both experimental data and mode-coupling-theory (MCT) predictions, aiming at a better understanding of structural relaxation in orthoterphenyl. We pay special attention to the wavenumber dependence of the collective dynamics. It is shown that the simulation results for the model share many features with experimental data for real system, and that MCT captures the simulation results at the semiquantitative level except for intermediate wavenumbers connected to the overall size of the molecule. Theoretical results at the intermediate wavenumber region are found to be improved by taking into account the spatial correlation of the molecule's geometrical center. This supports the idea that unusual dynamical properties at the intermediate wavenumbers, reported previously in simulation studies for the model and discernible in coherent neutron-scattering experimental data, are basically due to the coupling of the rotational motion to the geometrical-center dynamics. However, there still remain qualitative as well as quantitative discrepancies between theoretical prediction and corresponding simulation results at the intermediate wavenumbers, which call for further theoretical investigation.

PACS numbers: 61.20.Ja, 61.20.Lc, 61.25.Em, 64.70.Pf

## I. INTRODUCTION

Describing the microscopic origin of structural slowing down on cooling or compressing glass-forming liquids is one of the most challenging problems in condensed matter physics. During the past decade the research in this field was strongly influenced by the idealized mode-coupling theory (MCT) for the evolution of structural relaxation [1–3]. The theory predicts the structural arrest – also referred to as the idealized liquid-glass transition – driven by the mutual blocking of a particle and its neighbors (“cage effect”) at a critical temperature  $T_c$  which is located above the glass-transition temperature  $T_g$ . For temperatures close to but above  $T_c$ , MCT predicts universal scaling laws and power laws for describing the glassy slow structural relaxation. Although such complete structural arrest at  $T_c$  is not observed in experiments and therefore the idealized theory cannot literally be applied for describing dynamics below  $T_c$ , extensive tests of the theoretical predictions carried out so far against experimental and computer-simulation results suggest that MCT deals properly with some essential features of supercooled liquids [2, 3].

The molecular van der Waals liquid orthoterphenyl (OTP) has long been used as a model system in the study of the glass transition. (See, e.g., Refs. [4–6] and papers quoted therein.) Extensive experiments on OTP have been performed to monitor the onset of glassy structural relaxation on microscopic time and length scales. Using in particular quasielastic neutron scattering, the decay of

collective and self density fluctuations has been measured as a function of temperature, pressure, and wavenumber [4, 7–12]. Based on these studies, the validity of the *universal* predictions of MCT, such as the factorization theorem and the time-temperature superposition principle, has been established. However, there are *nonuniversal* aspects in the glassy structural relaxation which cannot be elucidated solely by those universal predictions. For example, parameters describing the decay of the collective density fluctuations in the  $\alpha$ -relaxation regime exhibit a characteristic wavenumber dependence, which is an important nonuniversal aspect to be accounted for by the theory [4, 12]. As will be discussed below, we found from the analysis of molecular-dynamics (MD) simulation results interesting dynamical properties of OTP at intermediate wavenumbers, and their theoretical investigation is one of the main points of the present paper.

One of the distinctive features of MCT is that it can also make predictions concerning nonuniversal aspects, such as the value of  $T_c$  and the details of the time and wavenumber dependence of various dynamical quantities, provided the system's static structure factor is known with sufficient accuracy. Utilizing this feature, there have been quantitative tests of the theory concerning nonuniversal as well as universal aspects using as input only the static structure factor determined from integral-equation theories or from computer simulations [13–19]. In the present paper, we apply MCT to discuss in detail properties of the slow structural relaxation in OTP, paying special attention to the wavenumber dependence of the structural  $\alpha$  relaxation of the collective dynamics. This will be done by regarding MD simulation results as a bridge connecting experimental data and theoretical predictions.

Although OTP is one of the simplest molecular sys-

---

\*Present address: Laboratoire de Physique Mathématique et Théorique, Université Montpellier II, 34095 Montpellier, France

tems from an experimental side, it is rather a complicated system for a theoretical treatment. Therefore, it is unavoidable to deal with a simple model for OTP which is still efficient in mimicking the complexity of the dynamical behavior of real system. In this respect, Lewis and Wahnström (LW) [20] introduced a particularly useful three-site model, each site playing the role of a whole phenyl ring, and this model will be considered in this paper.

For the LW OTP model, static and dynamic properties in supercooled states have been extensively studied based on MD simulations [21–23]. In the present work, the simulation results for the static structure factors serve as input to the theory, and those for dynamics can be used in testing the so-obtained theoretical results. Thereby, a stringent test of MCT predictions against the simulation results can be performed. Furthermore, by making connections between the simulation results for LW OTP and experimental ones for real system, the relevance of our theoretical results and their interpretation in understanding experimental data can be established.

A theoretical analysis for LW OTP has already been presented in Ref. [21] based on a simplified theory which is essentially the same as the one for spherical particles. But, since OTP is a molecular system, a full molecular approach is desirable. Recently, MCT for spherical particles has been extended to a theory for molecules. This has been done based on the tensor- and site-density formulations. In the tensor-density formulation, the density-fluctuation correlator is generalized to the one of infinite matrices of correlation functions formed with tensor-density fluctuations [17–19, 24–29]. However, the tensor-density formulation has the difficulty that the resulting equations are so involved, and it is not obvious whether those equations can be numerically solved within the regime of glassy dynamics. To overcome this difficulty, it has been suggested to base MCT for molecular systems on the site representation [30–34]. The fluctuations of the interaction-site densities have been used as the basic variables to describe the structure of the system. As a result, the known scalar MCT equations for the density fluctuations in simple systems have been generalized to  $n$ -by- $n$  matrix equations for the interaction-site-density fluctuations, where  $n$  denotes the number of atoms (or sites) forming the molecule. Thus, relatively simple equations of motions can be obtained within the site-representation, and these MCT equations will be solved in the present work to discuss the structural relaxation in OTP.

The paper is organized as follows. In Sec. II, the LW OTP model shall be introduced, and static as well as dynamic quantities to be used in discussions of simulation and theoretical results are defined. In Sec. III, MD-simulation results for LW OTP are summarized, and possible connections to the experimental results for real system are established. In Sec. IV, after reviewing relevant MCT equations based on the site representation, theoretical results are presented and compared with the

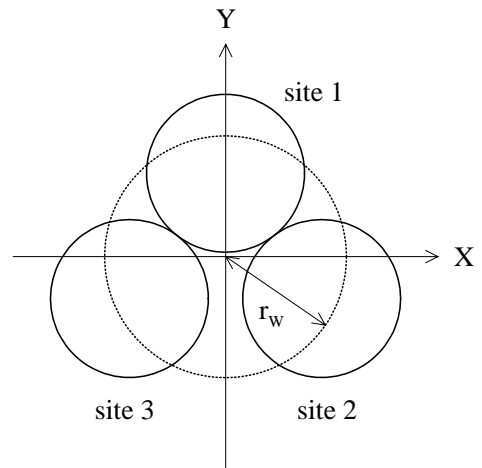


FIG. 1: Schematic representation of the three-site LW OTP molecule in the body-fixed molecular XY plane where the origin is taken to be the geometrical center (GC),  $\vec{r}_j^{\text{GC}} = (1/3) \sum_{a=1}^3 \vec{r}_j^a$ , and the Y axis is along the symmetry axis of the molecule. The diameter of each site is taken from the LJ parameter  $\sigma = 0.483$  nm. The dotted circle is drawn with the van der Waals radius  $r_w = 0.37$  nm [37] and taking GC as the origin.

simulation results. The paper is summarized in Sec. V with some concluding remarks.

## II. MODEL

The LW OTP molecule designed by Lewis and Wahnström [20] is a rigid isosceles triangle; the length of the two short sides of the triangle is  $\ell = 0.483$  nm and the angle between them is  $\theta = 75^\circ$ . Each of the three sites represents an entire phenyl ring of mass  $m \approx 78$  amu, and is described by a Lennard-Jones (LJ) sphere whose interaction potential is given by

$$V(r) = 4\epsilon[(\sigma/r)^{12} - (\sigma/r)^6] + A + Br, \quad (1)$$

with  $\epsilon = 5.276$  kJ/mol,  $\sigma = 0.483$  nm,  $A = 0.461$  kJ/mol, and  $B = -0.313$  kJ/(mol nm). Schematic representation of the LW OTP molecule is presented in Fig. 1. The shape of the molecule and the LJ parameters have been chosen to reproduce some bulk properties of the OTP molecule. The values of  $A$  and  $B$  are selected in such a way that the potential and its first derivative are zero at the cutoff  $r_c = 1.2616$  nm adopted in MD simulations. MD simulation results on the thermodynamic and dynamic properties of LW OTP have been reported in Refs. [20–23].

Discussions on the dynamics shall be done based on the site-site density correlators

$$F_q^{ab}(t) = \langle \rho_q^a(t) \rho_q^b(0) \rangle / N \quad (a, b = 1, 2, 3), \quad (2)$$

and their derivatives to be defined below. Here  $\rho_q^a(t) = \sum_{j=1}^N \exp[i\vec{q} \cdot \vec{r}_j^a(t)]$ , with  $\vec{r}_j^a(t)$  being the position vector of site  $a$  in  $j$ th molecule at time  $t$ , denotes the site-density fluctuations,  $N$  the number of molecules in the system, and  $\langle \dots \rangle$  canonical averaging for temperature  $T$ . (As depicted in Fig. 1, we shall use the convention that  $a = 1$  refers to the central site and  $a = 2, 3$  to the adjacent sites.) Because of isotropy,  $F_q^{ab}(t)$  depends only on the wavenumber  $q = |\vec{q}|$ . The initial values constitute the site-site static structure factors,  $S_q^{ab} = F_q^{ab}(0)$ , which provide the simplest information on the equilibrium structure of the system.

We also introduce tagged-molecule correlators,  $F_{q,s}^{ab}(t) = \langle \rho_{q,s}^a(t)^* \rho_{q,s}^b(0) \rangle$ , in which  $\rho_{q,s}^a(t) = \exp[i\vec{q} \cdot \vec{r}_s^a(t)]$  with  $\vec{r}_s^a(t)$  denoting the position vector of site  $a$  in the tagged molecule (labeled  $s$ ) at time  $t$ . The initial value shall be denoted as  $w_q^{ab} = F_{q,s}^{ab}(0)$ . For a rigid molecule, it is given by  $w_q^{ab} = \delta^{ab} + (1 - \delta^{ab})j_0(q l^{ab})$ , where  $j_0(x)$  denotes the 0th-order spherical Bessel function and  $l^{ab}$  the distance between sites  $a$  and  $b$ .

Let us consider a more convenient representation of the site-site density correlators which exploits the  $C_{2v}$  symmetry of the LW OTP molecule. For this purpose, we introduce the following density correlators

$$F_q^X(t) = \langle \rho_q^X(t)^* \rho_q^X(0) \rangle / N \text{ for } X = N, Z, \text{ and } Q, \quad (3)$$

defined in terms of the linear combinations

$$\begin{aligned} \rho_q^N &= (\rho_q^1 + \rho_q^2 + \rho_q^3) / \sqrt{3}, & \rho_q^Z &= (2\rho_q^1 - \rho_q^2 - \rho_q^3) / \sqrt{6}, \\ \rho_q^Q &= (\rho_q^2 - \rho_q^3) / \sqrt{2}, \end{aligned} \quad (4)$$

of the site-density fluctuations  $\rho_q^a$  ( $a = 1, 2$ , or  $3$ ). One can easily show that  $F_q^X(t)$  can be expressed in terms of  $F_q^{ab}(t)$ : one finds, for example,  $F_q^N(t) = \sum_{a,b=1}^3 F_q^{ab}(t)/3$ . Their normalized correlators shall be denoted as  $\phi_q^X(t) = F_q^X(t)/S_q^X$  with the corresponding static structure factor  $S_q^X = F_q^X(0)$ . We also introduce self-parts of these correlators, to be denoted as  $F_{q,s}^X(t)$ , which are defined similarly in terms of the site-density fluctuations  $\rho_{q,s}^a$  of the tagged molecule. Normalized tagged-molecule's correlators shall be written as  $\phi_{q,s}^X(t) = F_{q,s}^X(t)/w_q^X$  with  $w_q^X = F_{q,s}^X(0)$ .

Due to the  $C_{2v}$  symmetry of the LW OTP molecule, one finds that density correlators involving  $\rho_q^Q$ ,  $\langle \rho_q^X(t)^* \rho_q^Q \rangle / N$ , become nonzero only for  $X = Q$ , and the nonzero correlator for  $X = Q$  is identical to its self-part, i.e.,  $F_q^Q(t) = F_{q,s}^Q(t)$ . Viewed as a matrix, this means that  $\langle \rho_q^X(t)^* \rho_q^Y \rangle / N$  ( $X, Y = N, Z$ , or  $Q$ ) can be represented as

$$\begin{pmatrix} F_q^N(t) & F_q^{NZ}(t) & 0 \\ F_q^{NZ}(t) & F_q^Z(t) & 0 \\ 0 & 0 & F_q^Q(t) \end{pmatrix}, \quad (5)$$

where the only cross correlation is given by  $F_q^{NZ}(t) = \langle \rho_q^N(t)^* \rho_q^Z \rangle / N$ . Thus, the dynamics associated with the

variable  $Q$  is uncoupled from the one with  $N$  and  $Z$ , and is strictly connected to the single-molecule dynamics.

Assuming the equal scattering lengths for all the constituent sites, the normalized correlator  $\phi_q^N(t)$  is directly related to the cross section as measured in the coherent neutron scattering. The functional forms of  $\phi_q^Z(t)$  and  $\phi_q^Q(t)$  have been chosen so that their small-wavenumber limits reduce to the 1st-rank reorientational correlators [23] respectively for the directions associated with the  $Y$  and  $X$  axes in Fig. 1. Dynamical features of  $\phi_q^N(t)$  based on MD simulations have already been discussed in Refs. [21, 23], and some results on  $\phi_q^Z(t)$  and  $\phi_q^Q(t)$  in Ref. [23].

Two formulae shall be quoted here which are useful in analyzing simulation results for correlators. (For simplicity, we shall write down only those formulas for  $\phi_q^X(t)$ , but similar ones hold for all the correlators introduced above.) The correlator  $\phi_q^X(t)$  in supercooled states exhibits the two-step relaxation: the relaxation toward the plateau, followed by the final relaxation from the plateau to zero. The latter is referred to as the  $\alpha$ -relaxation. The von Schweidler law as derived from MCT including the next to leading order corrections [35]

$$\phi_q^X(t) = f_q^{Xc} - h_q^X (t/\tau)^b + h_q^{X(2)} (t/\tau)^{2b} + O((t/\tau)^{3b}), \quad (6)$$

describes the departure from the plateau value  $f_q^{Xc}$  – also referred to as the critical nonergodicity parameter – in the early  $\alpha$ -relaxation region. Here  $h_q^X$  and  $h_q^{X(2)}$  denote the critical and correction amplitudes, respectively,  $b$  the von Schweidler exponent, and  $\tau$  the  $\alpha$ -relaxation time. The exponent  $b$  is uniquely related to the so-called exponent parameter  $\lambda$  defined in MCT [1]. Another formula, which is purely empirical and well adopted for fitting correlators in the  $\alpha$ -relaxation region, is the Kohlrausch law

$$\phi_q^X(t) = A_q^X \exp[-(t/\tau_q^X)^{\beta_q^X}], \quad (7)$$

with the correlator-dependent  $\alpha$ -relaxation time  $\tau_q^X$  and the stretching exponent  $\beta_q^X$ . It is worthwhile to mention that, in the large- $q$  limit, the Kohlrausch law (7) can be derived from MCT [36]. In particular, one gets  $\lim_{q \rightarrow \infty} \beta_q^X = b$  irrespective of the choice for  $X$ . Since the exponent  $b$  is uniquely related to  $\lambda$ , the Kohlrausch-law fit in the large- $q$  regime thus provides a means to estimate  $\lambda$  based on simulation results for  $\phi_q^X(t)$ .

### III. SUMMARY OF SIMULATION RESULTS

In this section we summarize results of MD simulations performed for LW OTP: more complete description of the simulation results can be found in Refs. [21–23]. We also present some additional results which have not been considered so far. At the final subsection, we discuss that the simulation results for LW OTP share many features with experimental data for real system.

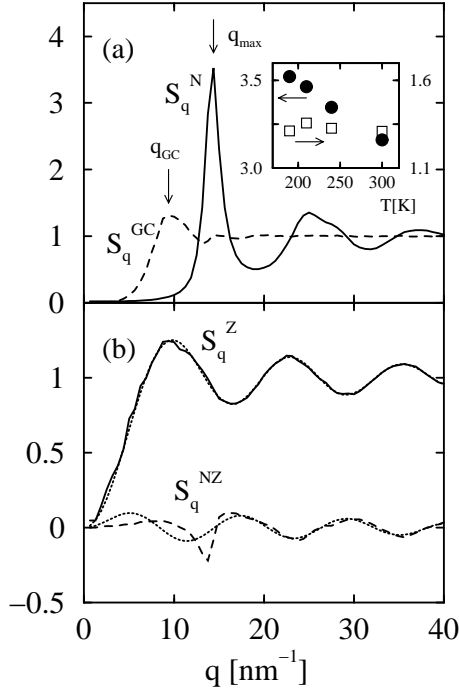


FIG. 2: MD simulation results for the static structure factors at  $\rho = 2.71$  molecules/nm<sup>3</sup> and  $T = 190$  K. (a) Solid and dashed lines respectively denote the static structure factor  $S_q^N$  and the geometrical-center static structure factor  $S_q^{GC}$ . In this and the following figures, the arrows indicate the peak positions  $q_{\max}$  ( $\approx 14.5$  nm<sup>-1</sup>) in  $S_q^N$  and  $q_{GC}$  ( $\approx 9$  nm<sup>-1</sup>) in  $S_q^{GC}$ . The inset exhibits the temperature dependence of the peak heights for  $S_q^N$  (filled circles, left scale) and  $S_q^{GC}$  (open squares, right scale). (b) Solid and dashed lines respectively denote the static structure factors  $S_q^Z$  and  $S_q^{NZ}$ . Dotted lines refer to their self-parts,  $w_q^Z$  and  $w_q^{NZ}$ .

### A. Static structure factors

We first briefly review the main features of the static structure factors, which turn out to be important in understanding simulation results for dynamics. These static structure factors are also to be used as input in theoretical calculations presented in Sec. IV.

Representative MD simulation results for the static structure factors in a supercooled state are presented in Figs. 2(a) and (b). We show in Fig. 2(a) the static structure factor  $S_q^N$  and the geometrical-center (GC) static structure factor  $S_q^{GC}$ . The latter is defined by  $S_q^{GC} = \sum_{j,l} \langle e^{-i\vec{q} \cdot (\vec{r}_j^{GC} - \vec{r}_l^{GC})} \rangle / N$  with  $\vec{r}_j^{GC}$  denoting the GC position  $\vec{r}_j^{GC} = (1/3) \sum_{a=1}^3 \vec{r}_j^a$  of the LW OTP molecule. The GC position actually coincides with the center-of-mass position, but we prefer to use the term “GC” because of the reason discussed in Ref. [23].  $S_q^N$  has a main peak at  $q = q_{\max}$  ( $\approx 14.5$  nm<sup>-1</sup>), which is compatible with the inverse of the LJ diameter  $\sigma = 0.483$  nm of a site in the sense that  $q_{\max} \sigma \approx 7$ . On the other hand,  $S_q^{GC}$

has a peak at  $q = q_{GC}$  ( $\approx 9$  nm<sup>-1</sup>) which can be related to the inverse of the van der Waals radius  $r_W = 0.37$  nm for OTP molecule [37] since  $q_{GC} \times (2r_W) \approx 7$ , i.e., it is connected to the overall size of the molecule (cf. Fig. 1).

Figure 2(b) exhibits the static structure factor  $S_q^Z$  and the cross correlation  $S_q^{NZ} = F_q^{NZ}(0)$ . Also added in this figure are their self-parts,  $w_q^Z$  and  $w_q^{NZ}$ . One recognizes that  $S_q^Z$  and  $w_q^Z$  are nearly the same. It is also seen that  $S_q^{NZ} \approx w_q^{NZ}$  holds to a reasonable extent, and that the magnitude of the cross correlation is rather small. This means that, within the description based on the site-site static structure factors, the representation (5) for  $t = 0$  is nearly diagonal, in which essentially only  $S_q^N$  is associated with the intermolecular correlation.

The peak at  $q = q_{GC}$  in  $S_q^{GC}$  also reflects intermolecular static correlations in the system. However, as discussed in Ref. [21] and reproduced in the inset of Fig. 2(a), the most pronounced temperature dependence in the static structure factors shows up at  $q = q_{\max}$  in  $S_q^N$ , whereas the peak at  $q = q_{GC}$  in  $S_q^{GC}$  is nearly temperature independent. Thus, for LW OTP, the slowing down of the dynamics upon lowering  $T$  is connected with the intermolecular correlation manifested as the main peak in  $S_q^N$  (the cage effect).

In the present work, we shall primarily be interested in the collective dynamics arising from intermolecular correlations. As noticed in connection with Eq. (5), the correlator  $\phi_q^Q(t)$  is strictly connected to the single-molecule dynamics,  $\phi_q^Q(t) = \phi_{q,s}^Q(t)$ . Furthermore,  $S_q^Z \approx w_q^Z$  and  $S_q^{NZ} \approx w_q^{NZ} \approx 0$  shown in Fig. 2(b) imply that also the correlator  $\phi_q^Z(t)$  approximately reflects the single-molecule dynamics only, i.e.,  $\phi_q^Z(t) \approx \phi_{q,s}^Z(t)$ . Indeed, we confirmed both from simulation and theoretical results that such approximation holds to a very good extent for the whole time region. We shall therefore not consider the correlators  $\phi_q^Z(t)$  and  $\phi_q^Q(t)$  any more in the following.

### B. Density dependence of $T_c$ and $\lambda$

Simulation results for the MCT critical temperature  $T_c$  and the exponent parameter  $\lambda$  are often determined from the fit of the diffusion constants  $D$  according to the MCT asymptotic power law [1]

$$D(T) \propto (T - T_c)^\gamma, \quad (8)$$

where the exponent  $\gamma$  is uniquely related to  $\lambda$ . Such a fit has been performed in Ref. [22] for various densities, and circles in Figs. 3(a) and (b) denote the resulting  $T_c$  and  $\lambda$  as a function of the density  $\rho$ . The critical temperature  $T_c$  increases with increasing  $\rho$ . The exponent parameter  $\lambda$  seems to increase with increasing  $\rho$ , but the statistical errors in simulations do not allow to rule out the possibility of a constant value (see below). We also notice that an unbiased three-parameter fit based on Eq. (8) suffers from correlations between the fit parameters  $T_c$

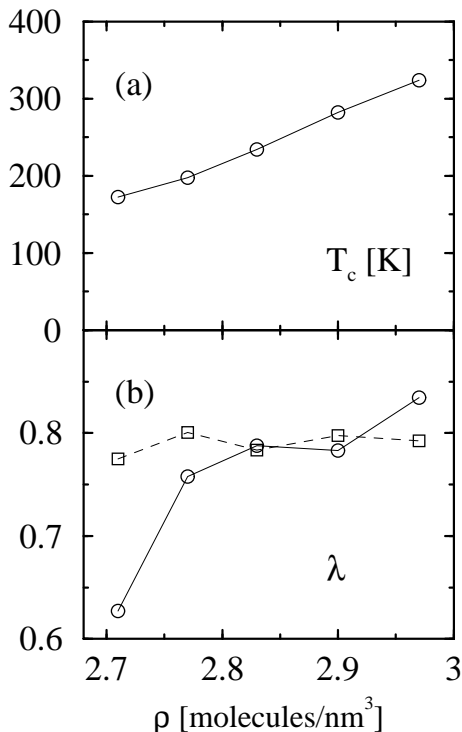


FIG. 3: MD simulation results for (a) the MCT critical temperature  $T_c$  and (b) the exponent parameter  $\lambda$  as a function of density  $\rho$ . Circles in (a) and (b) denote  $T_c$  and  $\lambda$  as determined from the fit of the diffusion constants  $D$  according to Eq. (8). In (b), squares refer to  $\lambda$  based on the exponent  $b$ , which is determined from the large- $q$  behavior of the density correlators  $\phi_q^N(t)$ . In both (a) and (b), lines are guide to the eyes.

and  $\gamma$  [14]. It also suffers from the identification of a fitting  $T$  range bounded below from  $T_c$  and above from the  $T$  at which correlation functions start to obey the time-temperature superposition. We note in passing that deviation from the MCT behavior for  $T < T_c$  has been discussed for the LW-OTP model in Ref. [22].

Often, the  $\rho$  dependence of  $T_c$  can be condensed into an effective coupling parameter

$$\Gamma \propto \rho T^{-1/4}. \quad (9)$$

This is the only relevant parameter for specifying the thermodynamic state of soft-sphere systems whose repulsive interaction is proportional to  $r^{-12}$  [38]. Indeed, in the case of binary mixture of soft spheres, it was found from computer simulations that the ideal glass transition occurs at a constant value,  $\Gamma = \Gamma_c$  [39, 40]. Although Eq. (9) is valid only for the  $r^{-12}$  soft-sphere system, a computer-simulation study for a model of polymer at different pressures [41] indicate that, also for LJ systems, the MCT critical point might be described well in terms of the effective coupling parameter. For LW OTP, we find from the  $\rho$  dependence of  $T_c$  shown in Fig. 3(a) that

$\Gamma_c = 1.57 \pm 0.05$ , where the prefactor in Eq. (9) has been chosen to be  $\sigma_\Gamma^3 \epsilon_\Gamma^{1/4}$  with  $\sigma_\Gamma = 0.76$  nm and  $\epsilon_\Gamma = 600$  K as in Ref. [11] for later comparison with experimental result. Thus, to a reasonable extent, the parameter  $\Gamma$  for LW OTP is also found to be nearly constant at the MCT critical point.

Concerning the  $\rho$  dependence of the exponent parameter  $\lambda$  shown in Fig. 3(b), we notice that a different value for  $\lambda$  is occasionally obtained from some other analysis of simulation results. For example, one gets another estimate for  $\lambda$  from the Kohlrausch-law fit of some density correlators as described just after Eq. (7).  $\lambda$  obtained in this way, based on the Kohlrausch-law fit of the correlators  $\phi_q^N(t)$ , are also included as squares in Fig. 3(b), which are nearly  $\rho$ -independent. (We confirmed that the stretching exponents in the large- $q$  regime do not depend on the choice of correlators.) The difference between circles and squares in Fig. 3(b) can be considered as a sort of error bars in determining  $\lambda$  based on the simulation results, but we already notice here that the insensitivity of  $\lambda$  to density is consistent with the experimental and theoretical results to be described below.

### C. Critical nonergodicity parameters and critical amplitudes

Figures 4(a) and (b) show the  $q$  dependence of the critical nonergodicity parameters  $f_q^{Nc}$  and the critical amplitudes  $h_q^N$  of the correlators  $\phi_q^N(t)$  based on the fit according to Eq. (6) for three representative densities,  $\rho = 2.71$ , 2.83, and 2.97 molecules/nm<sup>3</sup>. The fit of  $\phi_q^N(t)$  according to Eq. (6) has been performed by constraining the exponent  $b$  to the value specified by  $\lambda$ , the latter being taken from the squares in Fig. 3(b), and by regarding  $f_q^{Nc}$ ,  $h_q^N/\tau^b$  and  $h_q^{N(2)}/\tau^{2b}$  as fitting parameters. Thus,  $h_q^N$  and  $h_q^{N(2)}$  can be determined only up to  $q$ -independent multiplicative factors, and this is why  $h_q^N$  shown in Fig. 4(b) are given in arbitrary units. (Hence, one cannot directly compare the amplitude but only the wavevector dependence in  $h_q^N$  for different densities.)

For  $q \gtrsim q_{\max}$  ( $\approx 14.5$  nm<sup>-1</sup> for all the densities considered),  $f_q^{Nc}$  for the three densities are very similar to each other. For  $q < q_{\max}$ , on the other hand,  $f_q^{Nc}$  is higher for lower density, and this holds in particular around the intermediate wavenumber  $q_{GC}$  ( $\approx 9$  nm<sup>-1</sup>): whereas  $f_q^{Nc}$  at  $q \approx q_{GC}$  exhibits only a shoulder for the highest density  $\rho = 2.97$  molecules/nm<sup>3</sup>, a well-developed peak is discernible for the lowest density  $\rho = 2.71$  molecules/nm<sup>3</sup>.

The results for  $h_q^N$  shown in Fig. 4(b) are somewhat noisy compared to  $f_q^{Nc}$ . Concerning the  $q$  dependence, we notice that there are two minima in  $h_q^N$  located at  $q \approx q_{GC}$  and  $q_{\max}$ . As will be mentioned in Sec. III D, this is consistent with the existence of the peaks in  $f_q^{Nc}$  around these two wavenumbers. Furthermore, the minimum in  $h_q^N$  at  $q \approx q_{GC}$  is more pronounced for lower density in

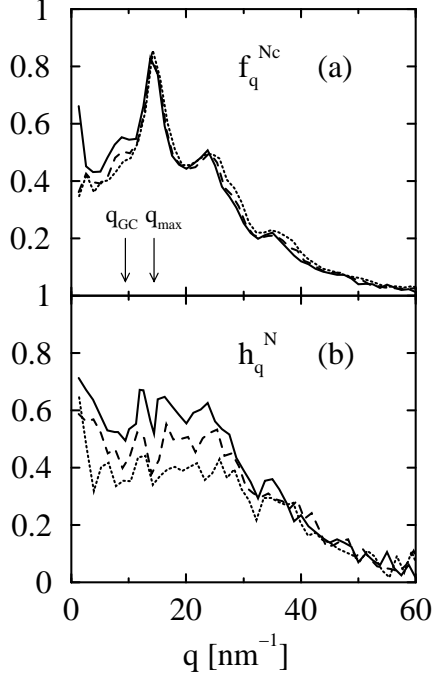


FIG. 4: MD simulation results for (a) the critical nonergodicity parameters  $f_q^{Nc}$  and (b) the critical amplitudes  $h_q^N$  of the correlators  $\phi_q^N(t)$  as determined from the fit according to Eq. (6) for three densities  $\rho = 2.71$  (solid lines), 2.83 (dashed lines), and 2.97 molecules/ $\text{nm}^3$  (dotted lines).  $h_q^N$  are in arbitrary units.

the sense that  $h_{q_{max}}^N/h_{q_{GC}}^N$  is larger for lower  $\rho$ , and this is also consistent with the found density dependence of  $f_q^{Nc}$  around this wavenumber.

#### D. Unusual feature in the wavenumber dependence

All parameters describing density correlations exhibit a characteristic wavenumber dependence reflecting that of the underlying static structure factor. As found in Ref. [21] and also discussed in more detail in Ref. [23], however, the dynamics in LW OTP exhibits an unusual wavenumber dependence of the critical nonergodicity parameters and the  $\alpha$ -relaxation times of the correlators  $\phi_q^N(t)$  at intermediate wavenumbers  $q \approx q_{GC}$ . Before embarking on the unusual feature, let us first consider a “usual” case as a reference.

We show in Figs. 5(a) and (b) the critical nonergodicity parameters  $f_q^c$ , the critical amplitudes  $h_q$ , the  $\alpha$ -relaxation times  $\tau_q$ , and the Kohlrausch stretching exponents  $\beta_q$  of normalized density correlators  $\phi_q(t)$  for the hard-sphere system as determined by solving the MCT equations for simple systems [1, 42].  $\tau_q$  and  $\beta_q$  have been obtained from the fit according to Eq. (7) of the  $\alpha$ -master curve for  $\phi_q(t)$ . The static structure factor used is evaluated within the Percus-Yevick approximation [38], and the one at the critical point is included in Fig. 5(a). A

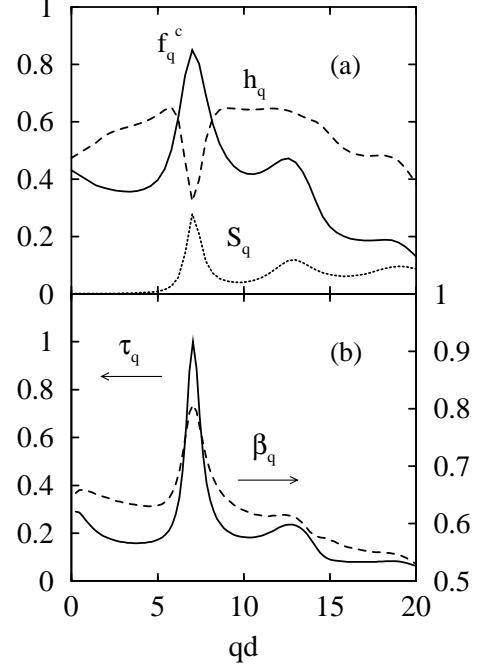


FIG. 5: MCT results for the wavenumber dependence of various quantities for the hard-sphere system as a function of  $qd$  with  $d$  denoting the hard-sphere diameter. (a) Solid and dashed lines respectively denote the critical nonergodicity parameters  $f_q^c$  and the critical amplitudes  $h_q$  for normalized density correlators  $\phi_q(t)$ . Dotted line refers to the Percus-Yevick static structure factor  $S_q$ , multiplied by a factor of 0.08 for ease of comparison, at the critical point. (b) Solid and dashed lines respectively denote the  $\alpha$ -relaxation times  $\tau_q$  and the stretching exponents  $\beta_q$  obtained from the fit according to Eq. (7) of the  $\alpha$ -master curve for  $\phi_q(t)$ .  $\tau_q$  are in arbitrary units.

strong correlation in the  $q$  dependence of these quantities can clearly be observed for the whole wavenumber regime:  $f_q^c$ ,  $1/h_q$ ,  $\tau_q$ , and  $\beta_q$  oscillate in phase with  $S_q$ , and this holds in particular around the first sharp diffraction peak,  $qd \approx 7$  with  $d$  denoting the hard-sphere diameter. A theoretical explanation of such correlation has already been documented [29, 35], and shall not be repeated here. Such “usual” results have been observed in simulation studies for LJ binary mixture [43], silica [44], and water [45], and also in experimental results reviewed in Ref. [46].

The result found in the simulation study for LW OTP is unusual in that such a correlation is violated at intermediate wavenumbers  $q \approx q_{GC}$ . This is summarized in Figs. 6(a) and (b) for the density  $\rho = 2.71$  molecules/ $\text{nm}^3$ . A related figure for  $\rho = 2.83$  molecules/ $\text{nm}^3$  can be found in Ref. [23]. One recognizes from Figs. 6(a) and (b) that  $f_q^{Nc}$ ,  $1/h_q^N$  and  $\tau_q^N$  of the correlator  $\phi_q^N(t)$  exhibit an additional peak at  $q \approx q_{GC}$  which does not exist in the corresponding static structure factor  $S_q^N$ . A signature of such a peak in  $\beta_q^N$  is also discernible, but a definitive conclusion cannot be drawn

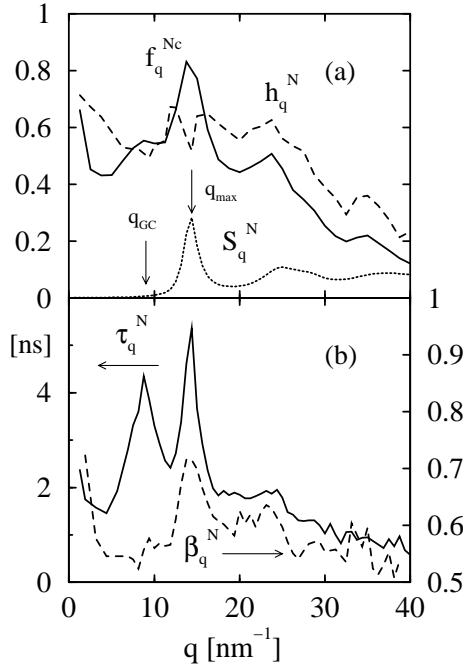


FIG. 6: MD simulation results for the wavenumber dependence of various quantities for LW OTP at  $\rho = 2.71$  molecules/nm<sup>3</sup>. (a) Solid and dashed lines respectively denote the critical nonergodicity parameters  $f_q^{Nc}$  and the critical amplitudes  $h_q^N$  for the correlators  $\phi_q^N(t)$ .  $h_q^N$  are in arbitrary units. Dotted line refers to the static structure factor  $S_q^N$ , multiplied by a factor of 0.08 for ease of comparison, at  $T = 190$  K. (cf.  $T_c \approx 172$  K for this density, see Fig. 3.) (b) Solid and dashed lines respectively denote the  $\alpha$ -relaxation times  $\tau_q$  and the stretching exponents  $\beta_q$  obtained from the fit according to Eq. (7) of the correlators  $\phi_q^N(t)$  at  $T = 190$  K.

since the results for  $\beta_q^N$  are rather noisy. As already noticed in connection with Figs. 4(a) and (b), this unusual feature is found to be more pronounced for lower density. It was suggested in Refs. [21, 23] that the unusual feature is caused by the coupling of the rotational motion to the GC motion. This follows from the fact that the GC static structure factor  $S_q^{GC}$  has a peak at  $q = q_{GC}$  as shown in Fig. 2(a).

To understand what is really the unusual feature, especially concerning  $f_q^{Nc}$  shown in Fig. 6(a), we go back to the original site-site density correlators  $F_q^{ab}(t)$ . Let us recall that  $\phi_q^N(t) = F_q^N(t)/S_q^N$  with  $F_q^N(t) = \sum_{a,b=1}^3 F_q^{ab}(t)/3$  and  $S_q^N = \sum_{a,b=1}^3 S_q^{ab}/3$ . Critical nonergodicity parameters  $F_q^{abc}$  of the correlators  $F_q^{ab}(t)$ , obtained similarly from the fit according to Eq. (6), and the site-site static structure factors  $S_q^{ab}$  are shown in Figs. 7(a) and (b), respectively. (Only the independent components in  $F_q^{abc}$  and  $S_q^{ab}$  are shown. The independent components, e.g., in the total nine  $S_q^{ab}$ , are  $S_q^{11}$ ,  $S_q^{12}$ ,  $S_q^{22}$ , and  $S_q^{23}$  due to the symmetry  $S_q^{ab} = S_q^{ba}$  as well as the  $C_{2v}$  symmetry of the LW OTP molecule.) It is seen from the comparison of Figs. 7(a) and (b) that the

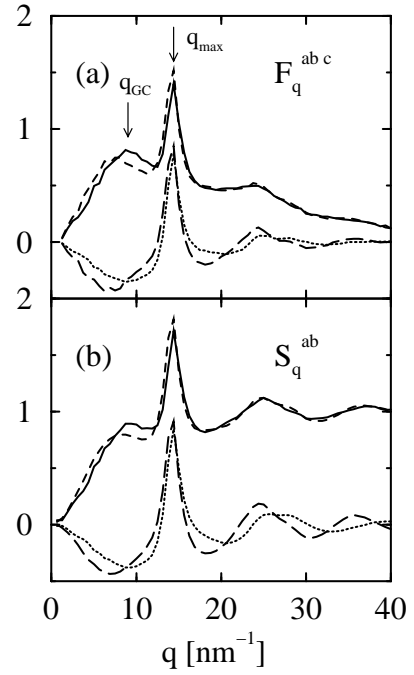


FIG. 7: MD simulation results for the site-site critical nonergodicity parameters  $F_q^{abc}$  and the site-site static structure factors  $S_q^{ab}$  for the density  $\rho = 2.71$  molecules/nm<sup>3</sup>. (a)  $F_q^{11c}$  (solid line),  $F_q^{12c}$  (dotted line),  $F_q^{22c}$  (dashed line), and  $F_q^{23c}$  (long-dashed line). (b)  $S_q^{11}$  (solid line),  $S_q^{12}$  (dotted line),  $S_q^{22}$  (dashed line), and  $S_q^{23}$  (long-dashed line) at  $T = 190$  K.

results for LW OTP are “usual” in the sense that the  $q$  dependence of  $F_q^{abc}$  correlates well with that of  $S_q^{ab}$  in the whole wavenumber regime including  $q \approx q_{GC}$ . We also notice that these quantities take positive and negative values at  $q \approx q_{GC}$ . The unusual feature concerning  $f_q^{Nc}$  shows up only after summing up the site-site  $F_q^{abc}$  and  $S_q^{ab}$  to obtain  $F_q^{Nc}$  and  $S_q^N$ . One observes that positive and negative components in  $S_q^{ab}$  almost cancel out after taking the summation, which results in small and flat  $S_q^N$  at  $q \approx q_{GC}$  as shown in Fig. 6(a). On the other hand, such a cancellation does not occur in the summation of the components  $F_q^{abc}$ , and this causes the unusual peak in  $F_q^{Nc}$ , and hence in  $f_q^{Nc} = F_q^{Nc}/S_q^N$ , at  $q \approx q_{GC}$ . Thus, the mentioned unusual feature reflects purely dynamical effects, since it can be observed only in such dynamical quantities as  $f_q^{Nc}$ ,  $1/h_q^N$  and  $\tau_q^N$ .

### E. Comparison with experimental results

Sine the LW OTP model is a very simplified one, one might think that a straightforward comparison of the MD simulation results with experimental data is not feasible. However, we discuss in the following that the simulation results for LW OTP share many features with experimental ones. Since we are interested in the  $q$  dependence

of collective dynamical quantities, especially in the vicinity of  $q_{GC}$  and  $q_{max}$ , we shall be mostly concerned with coherent neutron-scattering results. A review of neutron-scattering studies of OTP is presented in Ref. [5], and the experimental results to be presented below can be found in this article and references cited therein.

Let us first consider the static structure factor  $S_q^{exp}$  from coherent neutron scattering for fully deuterated OTP, which is given as a weighted sum of atomic correlations,  $S_q^{exp} \propto \sum_{\alpha,\beta} b_\alpha b_\beta S_q^{\alpha\beta}$ . Here  $\alpha$  and  $\beta$  refer to deuteron and carbon atoms,  $b_\alpha$  the scattering length, and  $S_q^{\alpha\beta}$  the partial structure factors. (Greek characters  $\alpha$  and  $\beta$  are used here to distinguish them from Roman characters  $a$  and  $b$  which have been adopted to label sites in the LW OTP molecule. Also, quantities as determined from experiments shall be distinguished with the superscript “exp”.) It has been observed that, in contrast to atomic systems, the main peak of  $S_q^{exp}$  is split into two maxima at about  $q = 14$  and  $19 \text{ nm}^{-1}$  [4]. Also, a shallow shoulder is discernible in  $S_q^{exp}$  around  $q = 9 \text{ nm}^{-1}$ . It was conjectured that the peak at  $q \approx 19 \text{ nm}^{-1}$  is built up mainly by intramolecular correlations within phenyl rings, while the maximum at  $q \approx 14 \text{ nm}^{-1}$  is associated with intermolecular correlations between phenyl rings. The shoulder at  $q \approx 9 \text{ nm}^{-1}$  was interpreted as being due to correlations between molecular centers of mass since its position is compatible with the inverse of the van der Waals radius  $r_W = 0.37 \text{ nm}$  [37].

This picture for  $S_q^{exp}$  is consistent with the simulation results for  $S_q^N$  and  $S_q^{GC}$  shown in Fig. 2(a). Since each site of the LW OTP molecule represents an entire phenyl ring, the peak at  $q_{max} \approx 14.5 \text{ nm}^{-1}$  in  $S_q^N$  corresponds to the first main peak in  $S_q^{exp}$ . No second peak around  $q \approx 19 \text{ nm}^{-1}$  can be observed in  $S_q^N$  since the internal structure within a phenyl ring is completely discarded in the LW OTP model. The peak at  $q_{GC} \approx 9 \text{ nm}^{-1}$  in  $S_q^{GC}$  is related to the shoulder in  $S_q^{exp}$ , although this is not reflected in  $S_q^N$ . As discussed in connection with Fig. 7(b), the disappearance of any shoulder or peak at  $q \approx q_{GC}$  in  $S_q^N$  is due to the cancellation of the constituent site-site correlation functions  $S_q^{ab}$ , which do exhibit (positive and negative) peaks around this wavenumber. Such an almost perfect cancellation might not occur in  $S_q^{exp}$ , due to more complicated nature of the constituent atomic correlations  $S_q^{\alpha\beta}$  in real system. Indeed, this conjecture is supported by MD-simulation studies for more realistic OTP models [47, 48], where a shoulder at  $q \approx 9 \text{ nm}^{-1}$  is discernible in the static structure factor which corresponds to  $S_q^{exp}$ .

It has been discussed for a liquid of linear molecules that orientational correlations can lead to a prepeak at low  $q$  [49]. By calculating the corresponding static orientational correlation functions, we confirmed that there is no prominent peak at  $q_{GC} \approx 9 \text{ nm}^{-1}$  in these functions for LW OTP. Therefore, we do not think the shoulder at  $q \approx 9 \text{ nm}^{-1}$  as observed in  $S_q^{exp}$  reflects the orientational correlations of the kind discussed in Ref. [49], and this is consistent with the picture that the shoulder stems from

the correlations between the molecular centers of mass.

We next compare the simulation and experimental results for the  $\rho$  dependence of  $T_c$  and  $\lambda$ . It has been shown in Ref. [11] from an analysis of incoherent density correlators at various pressures that the  $\rho$  dependence of  $T_c$  can be combined to the effective coupling parameter given in Eq. (9). This observation is in agreement with the simulation result for LW OTP. Furthermore, using the same prefactor as described just after Eq. (9), the experimental value  $\Gamma_c^{exp} \approx 1.498 \pm 0.004$  characterizing the MCT critical point is rather close to  $\Gamma_c \approx 1.57 \pm 0.05$  found for LW OTP. A smaller error bar in  $\Gamma_c^{exp}$  might be due to a narrower density range investigated in the experiment. Concerning  $\lambda$ , its insensitivity to density has been demonstrated with the experimental value  $\lambda^{exp} \approx 0.77$ . This is in accord with the simulation result shown as squares in Fig. 3(b), including the value for  $\lambda$ .

Coherent as well as incoherent neutron-scattering results for density correlators in supercooled states exhibit two-step relaxation in agreement with the prediction of MCT. The wavenumber dependence of various quantities characterizing such glassy dynamics has been determined from fits of those density correlators according to MCT asymptotic formulas or to the Kohlrausch law, like we did for simulation results. It was observed that the critical nonergodicity parameters  $f_q^{exp c}$  of coherent density correlators oscillate in phase with  $S_q^{exp}$ , with the two peaks around  $q_{GC}$  and  $q_{max}$  [4]. The critical amplitudes  $h_q^{exp}$  were found to oscillate in antiphase with  $S_q^{exp}$ , with the existence of two minima at  $q \approx q_{GC}$  and  $q_{max}$ . These trends are in agreement with the simulation results for  $\phi_q^N(t)$  shown in Fig. 6(a).

Let us now consider the  $q$  dependence of the relaxation times and the stretching exponents of coherent density correlators in the  $\alpha$ -relaxation regime. Some reservation is necessary in the experimental results for small  $q$  due to the presence of incoherent background and to contributions from multiple scattering. Therefore, the experimental  $\alpha$ -relaxation times  $\tau_q^{exp}$  show a tendency to increase for decreasing  $q$ . Nevertheless, on top of such background, it was observed that  $\tau_q^{exp}$  exhibit two plateaus around  $q_{GC}$  and  $q_{max}$  [12]. This is a signature of the characteristic  $q$  dependence as found in  $\tau_q^N$  for LW OTP shown in Fig. 6(b). Concerning the stretching exponents  $\beta_q^{exp}$ , a systematic variation in phase with  $S_q^{exp}$  was observed, especially in the vicinity of  $q_{max}$  [12], although a definitive conclusion cannot be drawn for  $q \approx q_{GC}$  due to the noise in the experimental results. Thus, the overall  $q$  dependence of  $\tau_q^{exp}$  and  $\beta_q^{exp}$  is in accord with the one for LW OTP shown in Fig. 6(b), and even a signature of the unusual peak at  $q \approx q_{GC}$  as discussed for LW OTP can be observed in  $\tau_q^{exp}$ .

A natural question arises as to whether the peaks at  $q \approx q_{GC}$  found in the experimental results for  $f_q^{exp c}$ ,  $1/h_q^{exp}$  and  $\tau_q^{exp}$  can really be considered as unusual. This is because, in contrast to  $S_q^N$  for LW OTP, the experimental static structure factor  $S_q^{exp}$  exhibits a shoulder, though tiny, in this wavenumber regime. However, it is



rather surprising that such a tiny shoulder in  $S_q^{\text{exp}}$  is related to a pronounced wavenumber variation of those dynamical quantities, and it seems worthwhile to pay special attention to dynamical features around  $q_{\text{GC}}$ . Therefore, we consider that a further investigation for the unusual features in LW OTP is valuable and might also be relevant in understanding the experimental results.

#### IV. THEORETICAL RESULTS

In this section, results for dynamical quantities calculated from MCT based on the site representation are presented, and are compared with those from the MD simulations. In particular, we examine whether the unusual feature at intermediate wavenumbers discussed in Sec. IIID can be accounted for by the theory. Since the unusual feature is found to be more pronounced for lower density, most of the theoretical calculations shall be done for the lowest density  $\rho = 2.71$  molecules/nm<sup>3</sup> studied in the MD simulations.

##### A. MCT equations based on the site representation

Within the site representation for molecules, the dynamics of the system is most naturally characterized by the site-site density correlators  $F_q^{ab}(t)$  defined for  $a, b = 1, \dots, n$ , where  $n$  denotes the number of sites in a molecule. The MCT equations for  $F_q^{ab}(t)$  consist of an exact Zwanzig-Mori equation and an approximate expression for the relaxation kernel, which are given in Ref. [33]. Regarding  $F_q^{ab}(t)$  as elements of an  $n \times n$  matrix  $\mathbf{F}_q(t)$ , the Zwanzig-Mori equation is given by

$$\partial_t^2 \mathbf{F}_q(t) + \Omega_q^2 \mathbf{F}_q(t) + \Omega_q^2 \int_0^t dt' \mathbf{m}_q(t-t') \partial_{t'} \mathbf{F}_q(t') = \mathbf{0}, \quad (10a)$$

where  $\Omega_q^2$  denotes the characteristic frequency matrix

$$\Omega_q^2 = q^2 \mathbf{J}_q \mathbf{S}_q^{-1}, \quad (10b)$$

with  $\mathbf{S}_q^{-1}$  representing the inverse matrix of  $\mathbf{S}_q$ .  $J_q^{ab}$  denote the site-site static (longitudinal) current correlation functions, whose explicit expressions for molecules possessing the  $C_{2v}$  symmetry (like LW OTP and water) in terms of molecule's inertia parameters can be found in Ref. [50]. The MCT expression for the relaxation kernel reads

$$\mathbf{m}_q(t) = \mathbf{S}_q \mathcal{F}_q[\mathbf{F}(t)], \quad (11a)$$

where the mode-coupling functional  $\mathcal{F}_q$  is given by the equilibrium quantities:

$$\mathcal{F}_q^{ab}[\tilde{\mathbf{f}}] = \frac{1}{2} \sum_{\lambda, \mu, \lambda', \mu'} \int d\vec{k} V_{\lambda\mu\lambda'\mu'}^{ab}(\vec{q}; \vec{k}, \vec{p}) \tilde{f}_k^{\lambda\mu} \tilde{f}_p^{\lambda'\mu'}, \quad (11b)$$

$$V_{\lambda\mu\lambda'\mu'}^{ab}(\vec{q}; \vec{k}, \vec{p}) = \frac{\rho}{(2\pi)^3} \{ \vec{q} \cdot [\delta^{a\lambda'} \vec{k} c_k^{a\lambda} + \delta^{a\lambda} \vec{p} c_p^{a\lambda'}] \} \\ \times \{ \vec{q} \cdot [\delta^{b\mu'} \vec{k} c_k^{b\mu} + \delta^{b\mu} \vec{p} c_p^{b\mu'}] \} / q^4, \quad (11c)$$

with  $\vec{p} = \vec{q} - \vec{k}$ . (We have used here a slightly different convention for writing the mode-coupling functional from the one adopted in Ref. [33] to simplify some equations which follow.) Here, the direct correlation function is defined via the site-site Ornstein-Zernike equation [38],  $\rho c_q^{ab} = [\mathbf{w}_q^{-1}]^{ab} - [\mathbf{S}_q^{-1}]^{ab}$ . Equations (10) and (11) constitute a set of closed equations of motion for determining  $\mathbf{F}_q(t)$ , provided the static structure factors  $S_q^{ab}$  are known. In the present work,  $S_q^{ab}$  determined from MD simulations shall be used.

The matrix of long-time limits (or the nonergodicity parameters),  $\mathbf{F}_q = \mathbf{F}_q(t \rightarrow \infty)$ , obeys the implicit equation defined by the mode-coupling functional  $\mathcal{F}_q$ ,

$$\mathbf{F}_q [\mathbf{S}_q - \mathbf{F}_q]^{-1} = \mathbf{S}_q \mathcal{F}_q[\mathbf{F}]. \quad (12)$$

This equation can be derived from Eqs. (10a) and (11a) by taking the  $t \rightarrow \infty$  limit. From an iterative procedure  $\mathbf{F}_q^{(j+1)}[\mathbf{S}_q - \mathbf{F}_q^{(j+1)}]^{-1} = \mathbf{S}_q \mathcal{F}_q[\mathbf{F}^{(j)}]$  starting with  $\mathbf{F}_q^{(0)} = \mathbf{S}_q$ , one obtains a solution of Eq. (12) as  $\mathbf{F}_q = \lim_{j \rightarrow \infty} \mathbf{F}_q^{(j)}$  [33]. One gets trivial solutions  $\mathbf{F}_q = \mathbf{0}$  for  $T > T_c$ , whereas nontrivial solutions  $\mathbf{F}_q \succ \mathbf{0}$  can be obtained for  $T \leq T_c$ . Here, and in the following, we mean by  $\mathbf{F}_q \succ \mathbf{0}$  (or  $F_q^{ab} \succ 0$ ) that the matrix  $\mathbf{F}_q$  is positive definite. Thus, one obtains  $T_c$  as the highest temperature at which there holds  $\mathbf{F}_q \succ \mathbf{0}$ , and the solution at this critical point provides the critical nonergodicity parameters  $\mathbf{F}_q^c$ .

The convergence of the iterative procedure for Eq. (12) is ruled by the spectral radius of a stability matrix, which can be defined from the mode-coupling functional  $\mathcal{F}_q$  as in the case of simple systems [1] and is given by

$$C_{qk}^{aba'b'} = \sum_p \sum_{\lambda, \mu, \lambda', \mu'} V_{\lambda\lambda'\mu\mu'}^{ab} : qkp \\ \times [\mathbf{S}_k - \mathbf{F}_k]^{\lambda a'} [\mathbf{S}_k - \mathbf{F}_k]^{\mu b'} F_p^{\lambda' \mu'}. \quad (13)$$

In deriving this expression from Eq. (11b), the wavevector integrals are converted into discrete sums by introducing some upper cutoff and using a grid of  $M$  equally spaced values for the wavenumbers. Thus, the wavenumber ( $q$ ,  $k$  and  $p$ ) can now be considered as a label for an array of  $M$  values. Correspondingly, the coefficients  $V_{\lambda\mu\lambda'\mu'}^{ab}(\vec{q}; \vec{k}, \vec{p})$  in Eq. (11b) are expressed as  $V_{\lambda\lambda'\mu\mu'}^{ab} : qkp$  in Eq. (13). The details of the transformation of the mode-coupling functional to a polynomial in the discretized variables can be found in Ref. [35].

For the notational simplicity, we introduce new indices  $i = (q, a, b)$  and  $j = (k, a', b')$  using the so-called dictionary order, which run from 1 to  $Mn^2$ . Then, the stability matrix given in Eq. (13) is simply denoted as  $C_{ij}$ . Unlike the case of simple systems for which the stability matrix is given by positive matrix [1], each element of  $C_{ij}$  can take positive and negative values. However,  $C_{ij}$  can be considered as a generalized positive matrix in the sense that it transforms a positive definite matrix into another one: if  $x_i \succ 0$  (meaning  $x_q^{ab} \succ 0$ ), then  $\sum_j C_{ij} x_j \succ 0$

and  $\sum_i x_i C_{ij} \succ 0$ . Such matrix  $C_{ij}$  has a nondegenerate maximum eigenvalue  $E \leq 1$ , and the corresponding right ( $e_i$ ) and left ( $\hat{e}_i$ ) eigenvectors can be chosen as  $e_i \succ 0$  and  $\hat{e}_i \succ 0$  [51]. The MCT critical point is characterized by  $E^c = 1$ . Let  $e_i$  and  $\hat{e}_i$  specifically denote the right and left eigenvectors, respectively, of the stability matrix  $C_{ij}^c$  at the critical point:  $\sum_j C_{ij}^c e_j = e_i$ ,  $\sum_i \hat{e}_i C_{ij}^c = \hat{e}_j$ . The eigenvectors are fixed uniquely by requiring  $\sum_i \hat{e}_i e_i = 1$  and  $\sum_i \hat{e}_i [\mathbf{e}(\mathbf{S} - \mathbf{F}^c)\mathbf{e}]_i = 1$ . These eigenvectors can be used to evaluate the critical amplitudes

$$\mathbf{H}_q = [\mathbf{S}_q - \mathbf{F}_q^c] \mathbf{e}_q [\mathbf{S}_q - \mathbf{F}_q^c], \quad (14)$$

and the exponent parameter  $\lambda$

$$\lambda = \sum_q \sum_{a,b} \hat{e}_q^{ab} \mathcal{F}_q^{ab}[\mathbf{H}]. \quad (15)$$

The above formulation for molecular systems is essentially the same as the one for simple systems, the only difference being the appearance of matrices in place of scalar quantities. It is then obvious that all the universal results concerning the MCT-liquid-glass-transition dynamics, as originally derived for simple systems [1], are valid also for MCT for molecular systems with such replacement of scalar quantities with matrices.

Since the LW OTP molecule consists of three sites, a natural choice would be  $n = 3$ , and the MCT equations (10) and (11) for this model are given by  $3 \times 3$  matrix equations. On the other hand, the analysis of the simulation results presented in Sec. III D concerning the unusual feature at intermediate  $q \approx q_{GC}$  suggests the importance of taking into account the spatial correlation of GC through the static structure factor  $S_q^{GC}$ . This implies that, in accounting for the unusual feature at  $q \approx q_{GC}$ , it might be necessary to include GC as the additional 4th site in the theoretical calculations. This leads to another formulation for LW OTP based on  $4 \times 4$ -matrix site-site density correlators  $F_q^{ab}(t)$ , for which the MCT equations (10) and (11) are given by  $4 \times 4$  matrix equations. The required static inputs  $S_q^{ab}$  for  $a, b = 1, \dots, 4$  in the new formulation can also be determined from MD simulations. By comparing theoretical results with and without including GC, one can judge whether the unusual feature at the intermediate wavenumbers  $q \approx q_{GC}$  discussed in Sec. III D stems from the coupling to the GC dynamics or not.

One might think that the inclusion of GC as an additional site is an ad hoc procedure, which is motivated in view of the simulation results. This kind of problems can occur in the site-density formulation since the site-density fluctuations  $\rho_q^a$  defined for *finite* number of sites do not provide a complete set of variables describing the dynamics of molecules. This is in contrast to the tensor-density fluctuations as adopted in Refs. [17–19, 24–29], which do provide a complete set of variables for molecules and also naturally incorporate the GC correlation. However, as mentioned in Sec. III A, the most important density fluctuations relevant for the structural slowing down

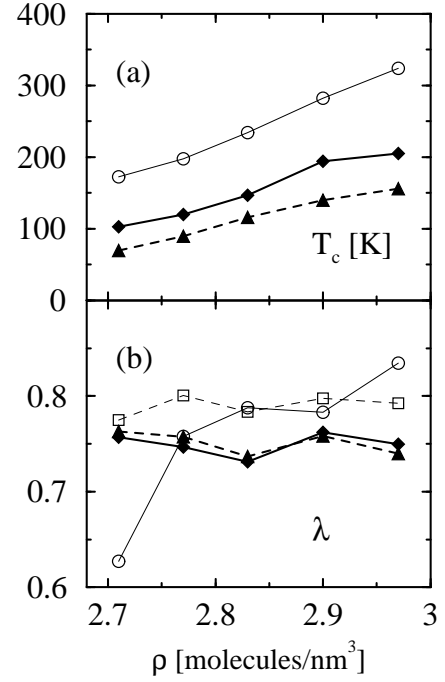


FIG. 8: Same as in Fig. 3, but here theoretical results are included as well. In both (a) and (b), MCT results with and without including GC are denoted as filled diamonds (connected with thick solid line) and filled triangles (connected with thick dashed line), respectively.

manifest themselves as the main peak at  $q = q_{\max}$  in  $S_q^N$  (the cage effect). Such correlations are incorporated in the site-density formulation even with the natural choice for the number of sites ( $n = 3$  for LW OTP). Indeed, it will be shown below that the MCT equations with  $n = 3$  can describe the basic feature of the simulation results, and this formulation is already useful. Our attitude here to include GC as an additional site (resulting in  $n = 4$ ) is only for the investigation of the dynamical features at  $q \approx q_{GC}$ . In fact, we will see that the inclusion of GC does not alter significantly the results for the wavenumbers other than  $q \approx q_{GC}$ .

## B. Density dependence of $T_c$ and $\lambda$

Figures 8(a) and (b) respectively show the theoretical results for  $T_c$  and  $\lambda$  as a function of the density  $\rho$ , along with the corresponding simulation results to be denoted as  $T_c^{\text{MD}}$  and  $\lambda^{\text{MD}}$  from here on in this section. It is seen from Fig. 8(a) that both of the theoretical  $T_c$ , with and without including GC, exhibit qualitatively the same density dependence as that of  $T_c^{\text{MD}}$ . Concerning  $\lambda$  shown in Fig. 8(b), the theoretical results with and without including GC are practically the same, and are nearly independent of  $\rho$ . The latter feature is in accord with the simulation result shown as squares in Fig. 8(b). The agreement between the theoretical and simulation

results for the value of  $\lambda$  is reasonable in view of the error bars in estimating  $\lambda^{\text{MD}}$  as discussed in connection with Fig. 3(b).

The theoretical  $T_c$  with including GC is in better agreement with  $T_c^{\text{MD}}$ , but is still located considerably below  $T_c^{\text{MD}}$  at all the densities investigated. One might think that the discrepancy between the theoretical  $T_c$  and  $T_c^{\text{MD}}$  is much larger than the one known for the hard-sphere system (HSS): MCT for HSS yields the critical packing fraction  $\varphi_c$  which differs only about 7% from the experimental value  $\varphi_c^{\text{exp}}$  for hard-sphere colloids [14], for which HSS is known to serve as a good model. (The previous estimate of the difference between the theoretical  $\varphi_c$  and the experimental  $\varphi_c^{\text{exp}}$  was about 15% [1], but a recent analysis performed in Ref. [14] indicates that half of this error is due to the use of the Percus-Yevick static structure factor as input instead of simulated one.) However, we argue in the following that the discrepancy between the theoretical  $T_c$  and  $T_c^{\text{MD}}$  for LW OTP is of comparable size to the one for HSS.

To this end, we notice that the  $\rho$  dependence of  $T_c^{\text{MD}}$  could be condensed into a nearly constant effective coupling parameter  $\Gamma_c^{\text{MD}} = 1.57 \pm 0.05$  (cf. Sec. III B). We found that, to a reasonable extent, this holds also for the theoretical results: from the  $\rho$  dependence of the theoretical  $T_c$ , one gets  $\Gamma_c = 1.77 \pm 0.07$  and  $1.9 \pm 0.1$  with and without including GC, respectively. Thus, in terms of the critical effective coupling parameter  $\Gamma_c$ , the discrepancies between the theoretical and simulation results are only within 13% and 20% with and without including GC, and are of comparable size to the discrepancy found for HSS. A similar analysis has been done for binary mixture of LJ particles (BMLJ) [15], for which it was discussed that the difference between  $T_c = 0.922$  from MCT and  $T_c^{\text{MD}} = 0.435$  from the MD simulation is comparable ( $\approx 20\%$ ) to the one for HSS when quantified in terms of the effective coupling parameter. We thus conclude that our theoretical estimate of  $T_c$  for LW OTP is within the comparable error bar as the one for HSS and BMLJ.

However, we notice that our theoretical results exhibit an unconventional feature in that  $T_c$  is *underestimated* compared to  $T_c^{\text{MD}}$ . This is in contrast to all previous MCT calculations, where MCT is found to overestimate  $T_c$  (or underestimate  $\varphi_c$  when the packing fraction is concerned): e.g.,  $\varphi_c = 0.546 < \varphi_c^{\text{exp}} \approx 0.58$  for HSS [14], and  $T_c = 0.922 > T_c^{\text{MD}} = 0.435$  for BMLJ [15]. In particular, this is also in contrast to MCT results for molecules based on the tensor-density formulation [17–19]. Concerning this problem, we notice that including the triple direct correlation function  $c_3$  was found to move up  $T_c$  for LW OTP more than by a factor of 2 [21]. Although the finding in Ref. [21] is based on the simplified scalar MCT equations dealing with the correlators  $\phi_q^N(t)$  only, we expect that the inclusion of  $c_3$  would significantly move up  $T_c$  shown in Fig. 8(a) and would lead to  $T_c > T_c^{\text{MD}}$  in agreement with the previous MCT studies.

Such theoretical calculations with including  $c_3$ , how-

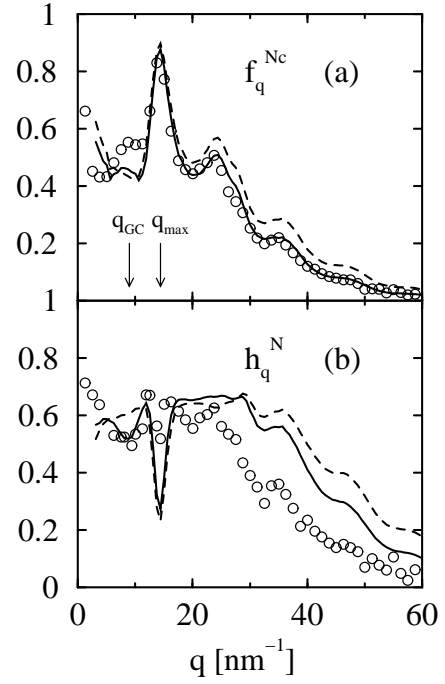


FIG. 9: Comparison of MD simulation and theoretical results for (a) the critical nonergodicity parameters  $f_q^{Nc}$  and (b) the critical amplitudes  $h_q^N$  of the correlators  $\phi_q^N(t)$  for the density  $\rho = 2.71$  molecules/nm<sup>3</sup>. In both (a) and (b), circles denote the simulation results as determined from the fit according to Eq. (6), while solid and dashed lines refer to MCT results with and without including GC, respectively. The simulation results for  $h_q^N$  are in arbitrary units.

ever, shall not be performed in the present work. This is basically because an accurate evaluation of  $c_3$  from MD simulations is quite a demanding task. Furthermore, it was also found in Ref. [21] for LW OTP that including  $c_3$  does not significantly alter theoretical results other than  $T_c$ , and we consider that MCT without  $c_3$  captures the essential physics in the dynamics of supercooled LW OTP. Indeed, as we will see below, our MCT results without the use of  $c_3$  are in semiquantitative agreement with the simulation results.

### C. Critical nonergodicity parameters and critical amplitudes

Figures 9(a) and (b) compare the theoretical and MD simulation results for the critical nonergodicity parameters  $f_q^{Nc}$  and the critical amplitudes  $h_q^N$  of the correlators  $\phi_q^N(t)$ , respectively. In both of these figures, solid and dashed lines respectively refer to the MCT results with and without including GC, while circles denote the simulation results.

Concerning  $f_q^{Nc}$  shown in Fig. 9(a), it is seen that, even without including GC, the  $q$  dependence of the simulation result is well reproduced by the theory, especially

for wavenumbers  $q \gtrsim q_{\max}$ . However, the theory without GC fails to reproduce the peak in  $f_q^{Nc}$  at  $q \approx q_{GC}$  found in the simulation result. This peak is reproduced by the theory which includes GC, although its magnitude is underestimated. Furthermore, the overall agreement with the simulation result becomes better also for  $q \gtrsim q_{\max}$  by including GC.

Also for  $h_q^N$  exhibited in Fig. 9(b), the overall  $q$  dependence of the simulation result is well reproduced even by the theory without GC. On the other hand, the minimum in  $h_q^N$  at  $q \approx q_{GC}$  found in the simulation result is accounted for only by the theory which includes GC. The found improvement in the theoretical results for  $f_q^{Nc}$  and  $h_q^N$  at  $q \approx q_{GC}$ , which is achieved by including GC, supports the idea that the unusual wavenumber dependence discussed in Sec. IIID is basically due to the coupling to the GC dynamics. A further support shall be discussed in Sec. IVD from the analysis of the  $\alpha$ -relaxation times.

#### D. Dynamics in the $\alpha$ -relaxation region

As discussed in Ref. [23] for LW OTP based on the MD simulation, the most faithful tests of MCT concerning the dynamics should be performed in the  $\alpha$ -relaxation part starting from the plateau regime. This is because the approach toward the plateau, for which MCT predicts an asymptotic power-law  $\sim t^{-a}$  ( $0 < a < 0.5$ ) [1], was found to be almost completely masked by the microscopic dynamics. In view of this, tests of the theoretical results for density correlators shall be done in terms of MCT  $\alpha$ -master curves. Of particular relevance here is the MCT second scaling law – also referred to as the superposition principle – which states that correlators in the  $\alpha$ -relaxation region for different temperatures can be superposed on top of each other simply by rescaling the time scale:

$$\phi_q^X(t) = \tilde{\phi}_q^X(t/\tau_q^X). \quad (16)$$

Here  $\tilde{\phi}_q^X(\tilde{t})$  denotes the  $\alpha$ -master function.

In the strict test of the MCT second scaling law, on the other hand, one cannot freely choose the scale  $\tau_q^X$ , which can depend on the choice of the variable  $X$  as well as on the wavenumber  $q$ . According to MCT, there exists a single time scale, say  $\tau$ , characterizing the  $\alpha$  relaxation of all the correlators [1]. Thus, instead of Eq. (16), one actually has for the MCT second scaling law

$$\phi_q^X(t) = \tilde{\phi}_q^X(t/\tau). \quad (17)$$

The MCT  $\alpha$ -master function  $\tilde{\phi}_q^X(\tilde{t})$  can be evaluated from the MCT equations at  $T = T_c$  up to an overall time scale, with the initial behavior given by the von Schweidler law, Eq. (6) [1].

The mentioned second scaling law of MCT implies that the test of the MCT  $\alpha$ -master functions against simulation results for density correlators should be done

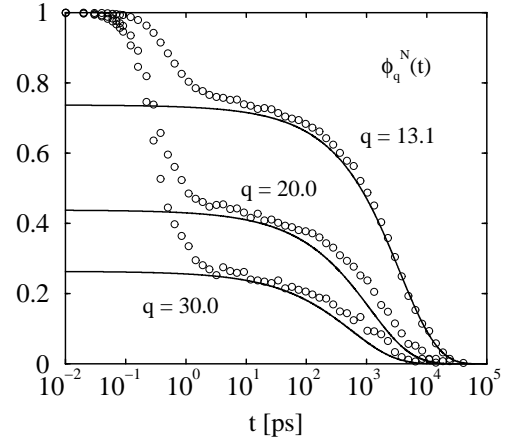


FIG. 10: Comparison of MD simulation and theoretical results for the correlators  $\phi_q^N(t)$  for the density  $\rho = 2.71$  molecules/nm<sup>3</sup> at three wavenumbers  $q = 13.1$ ,  $20.0$ , and  $30.0$  nm<sup>-1</sup>. Circles denote the simulation results at  $T = 190$  K. Solid lines refer to the  $\alpha$ -master curves  $\tilde{\phi}_q^N(t/\tau)$  from MCT including GC, where  $\tau$  has been chosen so that both the simulation and theoretical curves at  $q = 13.1$  nm<sup>-1</sup> yield the same  $\alpha$ -relaxation time  $\tau_q^N$  when fitted with Eq. (7).

by adjusting the single time scale  $\tau$  only. Such test is performed in Fig. 10 for the correlators  $\phi_q^N(t)$  at three wavenumbers  $q = 13.1$ ,  $20.0$ , and  $30.0$  nm<sup>-1</sup>, which are close to the first peak, the first minimum, and the second minimum in  $S_q^N$ , respectively (*cf.* Fig. 2). In Fig. 10, circles refer to the simulation results for  $\phi_q^N(t)$  at  $\rho = 2.71$  molecules/nm<sup>3</sup> and  $T = 190$  K. Solid lines denote the  $\alpha$ -master curves  $\tilde{\phi}_q^N(t/\tau)$  from MCT which includes GC, where  $\tau$  has been chosen so that both the theoretical and simulation curves at  $q = 13.1$  nm<sup>-1</sup> yield the same  $\alpha$ -relaxation time  $\tau_q^N$  when fitted with Eq. (7). It is seen from Fig. 10 that the MCT  $\alpha$ -master curves describe well the time dependence of the simulation results for  $\phi_q^N(t)$  in the  $\alpha$ -relaxation region, including the relative  $\alpha$ -relaxation times for different wavenumbers. (Notice that, from the construction of  $\tau$ , the real test of the relative  $\alpha$ -relaxation times is performed only for  $q = 20.0$  and  $30.0$  nm<sup>-1</sup> in Fig. 10.) In particular, the relaxation stretching, which is pronounced for  $q = 20.0$  and  $30.0$  nm<sup>-1</sup>, is well reproduced by the theory. Indeed, from the Kohlrausch-law fit according to Eq. (7), we found, e.g., for  $q = 20.0$  nm<sup>-1</sup>,  $\beta_q^N = 0.62$  from the MCT  $\alpha$ -master function and  $0.60$  from the simulation curve. A similar quantitative test of MCT against simulation results for density correlators, which uses the single time scale as an adjustable parameter, has been performed in Ref. [52] for binary mixture of LJ particles.

Theoretical and simulation results for the  $\alpha$ -relaxation times  $\tau_q^N$  and the stretching exponents  $\beta_q^N$  of the correlators  $\phi_q^N(t)$  for the whole wavenumbers are compared in Figs. 11(a) and (b), respectively, which are obtained from the fits according to Eq. (7). In these figures, solid and

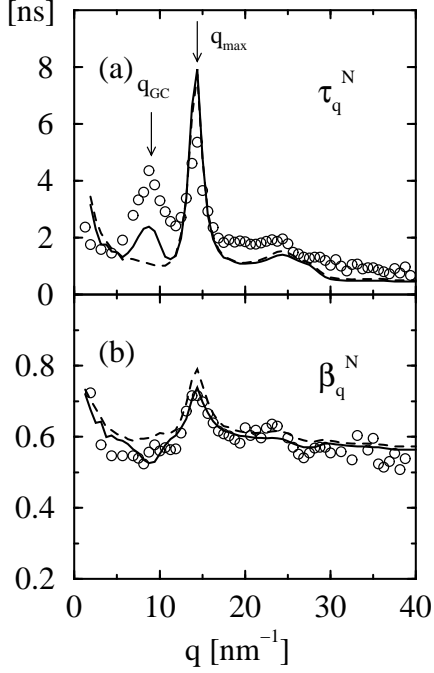


FIG. 11: Comparison of MD simulation and theoretical results for (a) the  $\alpha$ -relaxation times  $\tau_q^N$  and (b) the stretching exponents  $\beta_q^N$  of the correlators  $\phi_q^N(t)$  for the density  $\rho = 2.71$  molecules/nm<sup>3</sup>. In both (a) and (b), circles denote the simulation results at  $T = 190$  K, while solid and dashed lines refer to results from the MCT  $\alpha$ -master curves with and without including GC, respectively. The overall time scale of the theoretical results for  $\tau_q^N$  has been chosen so as to reproduce the same  $\tau_q^N$  at  $q = 13.1$  nm<sup>-1</sup> as that from the MD simulation.

dashed lines respectively denote the MCT results with and without including GC, whereas circles refer to the simulation results. Again, the overall scale of the theoretical results for the  $\alpha$ -relaxation times has been chosen so as to reproduce the same  $\tau_q^N$  at  $q = 13.1$  nm<sup>-1</sup> as that from the MD simulation. It is seen that, even without including GC, the  $q$  dependence of the simulation results for  $\tau_q^N$  and  $\beta_q^N$  is well reproduced by the theory at the semiquantitative level, especially for the wavenumbers  $q \gtrsim q_{\max}$ . For  $q < q_{\max}$ , on the other hand, it is seen from Fig. 11(a) that the unusual peak in the  $\alpha$ -relaxation times at intermediate  $q \approx q_{GC}$ , as observed in the simulation result, is reproduced only by the theory which includes GC, although its magnitude is still underestimated. This again supports the idea that the unusual peak is basically due to the coupling to the GC dynamics.

## V. SUMMARY AND CONCLUDING REMARKS

In this paper, we reported MD simulation results performed for a model of molecular liquid OTP developed

by Lewis and Wahnström, paying special attention to the wavenumber dependence of the structural  $\alpha$  relaxation of the collective dynamics, and showed that the simulation results for the model share many features with experimental data for real system (Sec. III). We then demonstrated that theoretical results based on MCT captures the simulation results at the semiquantitative level (Sec. IV): it is found that MCT yields a fair estimate of the critical temperature  $T_c$  and the exponent parameter  $\lambda$  including their density dependence, and predicts the wavenumber dependence of dynamical quantities rather well, in particular near the first sharp diffraction peak  $q_{\max}$  of the static structure factor  $S_q^N$ . Through these investigations, we established the relevance of our theoretical results and their interpretation in understanding experimental data for real system.

As described in Sec. III A, major intermolecular correlations manifest themselves as the peaks at  $q = q_{\max}$  in  $S_q^N$  and at  $q = q_{GC}$  in  $S_q^{GC}$ . On the other hand, the most pronounced temperature dependence in the static structure factors shows up at  $q = q_{\max}$  in  $S_q^N$  (cf. the inset of Fig. 2(a)). This indicates that the structural slowing down and anomalous glassy features in the dynamics upon lowering  $T$  are primarily caused by the intermolecular correlation manifested as the main peak in  $S_q^N$  (the cage effect). This is supported by the observation in Sec. IV that the theoretical results, which do not take into account  $S_q^{GC}$ , already capture the basic features of the simulation results.

On the other hand, though of subordinate nature in the above sense, the simulation results for LW OTP exhibit interesting and unusual properties at intermediate wavenumbers  $q \approx q_{GC}$ , which reflect purely dynamical effects. As discussed in Sec. III E, similar features can also be observed in experimental data for real system. We argued that such unusual features for  $q \approx q_{GC}$  are basically due to the coupling to the GC dynamics. This is because, compared to the simulation results, the theoretical results for  $q \approx q_{GC}$  were found to be improved by including the spatial correlation of GC through  $S_q^{GC}$ . However, there still remain quantitative discrepancies between the theoretical and simulation results for  $q \approx q_{GC}$  compared with the agreement found for the other wavenumber regime. This implies that the present theory still lacks some features which might be relevant for the dynamics at intermediate wavenumbers  $q \approx q_{GC}$ . Now, we provide additional evidence showing that this is the case.

Figure 12(a) exhibits the simulation result for the temperature dependence of the  $\alpha$ -relaxation times normalized by the one at  $q = q_{\max}$ ,  $\tau_q^N / \tau_{q_{\max}}^N$ , of the density correlators  $\phi_q^N(t)$  for the density  $\rho = 2.83$  molecules/nm<sup>3</sup>. MCT predicts the universal asymptotic power-law increase of the  $\alpha$ -relaxation times [1]. This implies that the ratio of the  $\alpha$ -relaxation times like the one shown in Fig. 12(a) should be temperature independent for  $T$  close to but above  $T_c$ , which is referred to as the  $\alpha$ -relaxation-scale coupling. However, Fig. 12(a) clearly demonstrates that this universal prediction of MCT is violated around

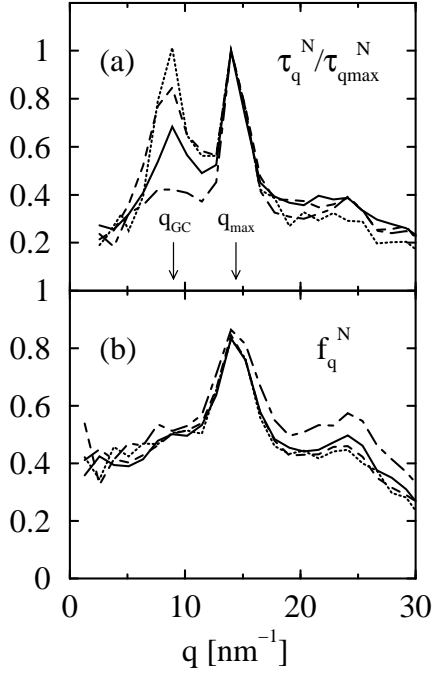


FIG. 12: MD simulation results for (a) the rescaled  $\alpha$ -relaxation times  $\tau_q^N / \tau_{q_{\max}}^N$  and (b) the plateau heights  $f_q^N$  of the correlators  $\phi_q^N(t)$  for the density  $\rho = 2.83$  molecules/nm<sup>3</sup>. The results at  $T = 260$  K (solid lines), 300 K (dashed lines), and 340 K (dotted lines) refer to  $T > T_c \approx 234$  K (cf. Fig. 3), whereas those at  $T = 230$  K (dash-dotted lines) to  $T < T_c$ .

(and only around) the wavenumber  $q_{GC}$ . (For the other wavenumbers, it is seen that the  $\alpha$ -relaxation-scale coupling holds fairly well, including  $T = 230$  K which is below  $T_c \approx 234$  K for the density considered.) Thus, the found temperature dependence of the ratio  $\tau_q^N / \tau_{q_{\max}}^N$  around  $q = q_{GC}$  is beyond the implication of MCT, and the present theory, formulated within the framework of MCT, cannot be used to explain such a finding. Unfortunately, due to the presence of incoherent background, it is not clear whether experimental results for the coherent  $\alpha$ -relaxation times reported in Ref. [12] also exhibit such a temperature dependence at  $q \approx q_{GC}$ . (See also below for some other related simulation and experimental studies.)

Combining the results shown in Figs. 4(a), 4(b) and 12(a), one recognizes another interesting property of the unusual peak at  $q \approx q_{GC}$  that it is more pronounced at *lower* density and at *higher* temperature. In view of the fact that the overall shape of the LW OTP molecule is well described as a sphere of the van der Waals radius  $r_W = 0.37$  nm (cf. Fig. 1), the dynamics at low-density, high-temperature regime is expected to be dominated by the spatial correlation of molecule's geometrical center, i.e., by  $S_q^{GC}$ . This is in contrast to the high-density, low-temperature glassy regime where the dynamics is primarily determined by the cage effect manifested as the main peak in  $S_q^N$ . Thus, one might conjecture that

the unusual feature at  $q \approx q_{GC}$  is an inheritance from the low-density, high-temperature dynamics, and that this cannot be explained by the universal predictions of MCT since, up to the lowest temperature investigated, the dynamics at  $q \approx q_{GC}$  might not have yet reached the asymptotic regime for which those MCT predictions are applicable. Such a possibility has been discussed in Refs. [29, 34], where the standard MCT scenario for the glass-transition dynamics was shown to be modified for some reorientational correlators due to precursor phenomena of a nearby type-A transition.

The above conjecture, however, might not be appropriate in the present case in view of the following result. Figure 12(b) exhibits the temperature dependence of the plateau heights  $f_q^N$  of the correlators  $\phi_q^N(t)$ . For  $T > T_c$ , the plateau height can be obtained from the von-Schweidler-law fit according to Eq. (6). Although Eq. (6) cannot be employed for fitting the correlators referring to  $T < T_c$ , we used it just to estimate the plateau heights  $f_q^N$  for  $T = 230$  K. (For  $T = 230$  K, the correlators  $\phi_q^N(t)$  exhibit well developed plateau regime as, e.g., shown in Fig. 3 of Ref. [23], and the plateau heights can easily be estimated from such graphs. We confirmed that the so-estimated plateau heights are in good agreement with the ones based on the ad-hoc use of the von-Schweidler-law fit.)

Since the plateau heights for  $T > T_c$  corresponds to the critical nonergodicity parameters  $f_q^{Nc}$  (cf. Eq. (6)), MCT predicts that they should be temperature independent. Furthermore, MCT predicts for  $T < T_c$  the increase of the plateau height,  $f_q^N - f_q^{Nc} \propto h_q^N > 0$ . The results shown in Fig. 12(b) are, within the statistical errors, consistent with these universal predictions of MCT. Notice that this holds also for the intermediate wavenumbers  $q \approx q_{GC}$ . Thus, the plateau heights around  $q = q_{GC}$  have already reached the asymptotic regime for which the universal MCT description is adequate. Since the plateau heights also quantify the strengths of the  $\alpha$ -relaxation processes, it is then difficult to imagine that only the  $\alpha$ -relaxation times have not yet reached the MCT asymptotic regime, and the above conjecture introduced to explain the finding in Fig. 12(a) might not be appropriate.

The position  $q \approx q_{GC}$  where the unusual feature we discussed occurs in LW OTP is compatible with the inverse of its van der Waals radius (cf. Sec. III A), i.e., it is connected to the overall size of the molecule. It is interesting to note that similar unusual peaks were found in a model for polymer around the intermediate wavenumber  $q = 2\pi/R_g$ , where  $R_g$  denotes the radius of gyration [53]: in this wavenumber regime, a shoulder is discernible in the critical nonergodicity parameters  $f_q^c$ , and peaks are observable in the inverse of the critical amplitudes  $1/h_q$ , the  $\alpha$ -relaxation times  $\tau_q$ , and the stretching exponents  $\beta_q$  of the correlators which correspond to  $\phi_q^N(t)$  in the present paper. In particular, the ratio  $\tau_q / \tau_{q_{\max}}$  of the  $\alpha$ -relaxation times at  $q \approx 2\pi/R_g$  for this model exhibits the same temperature dependence as the one shown in Fig. 12(a). A similar temperature dependence of the ra-

tio  $\tau_q/\tau_{q_{\max}}$  at intermediate  $q$  range ( $\approx 0.4 q_{\max}$ ) was also found in the coherent neutron scattering results for a real polymer system [54]. Thus, further investigations are necessary for a comprehensive understanding of the unusual features at intermediate wavenumbers as observed in simulation and experimental results for molecular and polymer systems.

## Acknowledgments

We thank H. Z. Cummins, W. Kob, and W. Götze for discussions and suggestions. We acknowledge support from MIUR COFIN and FIRB and from INFN PRA-GENFDT.

- 
- [1] W. Götze, in *Liquids, Freezing and Glass Transition*, edited by J.-P. Hansen, D. Levesque, and J. Zinn-Justin (North-Holland, Amsterdam, 1991), p. 287.
  - [2] W. Götze and L. Sjögren, Rep. Prog. Phys. **55**, 241 (1992).
  - [3] W. Götze, J. Phys.: Condensed Matter **11**, A1 (1999).
  - [4] A. Tölle, H. Schober, J. Wuttke, and F. Fujara, Phys. Rev. E **56**, 809 (1997).
  - [5] A. Tölle, Rep. Prog. Phys. **64**, 1473 (2001).
  - [6] G. Monaco, D. Fioretto, L. Comez, and G. Ruocco, Phys. Rev. E **63**, 061502 (2001).
  - [7] W. Petry, E. Bartsch, F. Fujara, M. Kiebel, H. Sillescu, and B. Farago, Z. Phys. B **83**, 175 (1991).
  - [8] M. Kiebel, E. Bartsch, O. Debus, F. Fujara, W. Petry, and H. Sillescu, Phys. Rev. B **45**, 10301 (1992).
  - [9] J. Wuttke, M. Kiebel, E. Bartsch, F. Fujara, W. Petry, and H. Sillescu, Z. Phys. B **91**, 357 (1993).
  - [10] E. Bartsch, F. Fujara, J. F. Legrand, W. Petry, H. Sillescu, and J. Wuttke, Phys. Rev. E **52**, 738 (1995).
  - [11] A. Tölle, H. Schober, J. Wuttke, O. G. Randl, and F. Fujara, Phys. Rev. Lett. **80**, 2374 (1998).
  - [12] A. Tölle, J. Wuttke, H. Schober, O. G. Randl, and F. Fujara, Eur. Phys. J. B **5**, 231 (1998).
  - [13] W. Götze and L. Sjögren, Phys. Rev. A **43**, 5442 (1991).
  - [14] G. Foffi, W. Götze, F. Sciortino, P. Tartaglia, and Th. Voigtmann, e-print cond-mat/0309007.
  - [15] M. Nauroth and W. Kob, Phys. Rev. E **55**, 657 (1997).
  - [16] F. Sciortino and W. Kob, Phys. Rev. Lett. **86**, 648 (2001).
  - [17] A. Winkler, A. Latz, R. Schilling, and C. Theis, Phys. Rev. E **62**, 8004 (2000).
  - [18] L. Fabbian, A. Latz, R. Schilling, F. Sciortino, P. Tartaglia, and C. Theis, Phys. Rev. E **60**, 5768 (1999).
  - [19] C. Theis, F. Sciortino, A. Latz, R. Schilling, and P. Tartaglia, Phys. Rev. E **62**, 1856 (2000).
  - [20] L. J. Lewis and G. Wahnström, Phys. Rev. E **50**, 3865 (1994).
  - [21] A. Rinaldi, F. Sciortino, and P. Tartaglia, Phys. Rev. E **63**, 061210 (2001).
  - [22] S. Mossa, E. La Nave, H. E. Stanley, C. Donati, F. Sciortino, and P. Tartaglia, Phys. Rev. E **65**, 041205 (2002).
  - [23] S.-H. Chong and F. Sciortino, Europhys. Lett. **64**, 197 (2003).
  - [24] R. Schilling and T. Scheidsteger, Phys. Rev. E **56**, 2932 (1997).
  - [25] C. Theis and R. Schilling, J. Non-Cryst. Solids **235–237**, 106 (1998).
  - [26] M. Letz, R. Schilling, and A. Latz, Phys. Rev. E **62**, 5173 (2000).
  - [27] T. Theenhaus, R. Schilling, A. Latz, and M. Letz, Phys. Rev. E **64**, 051505 (2001).
  - [28] T. Franosch, M. Fuchs, W. Götze, M. R. Mayr, and A. P. Singh, Phys. Rev. E **56**, 5659 (1997).
  - [29] W. Götze, A. P. Singh, and Th. Voigtmann, Phys. Rev. E **61**, 6934 (2000).
  - [30] S.-H. Chong and F. Hirata, Phys. Rev. E **58**, 6188 (1998).
  - [31] S.-H. Chong, W. Götze, and A. P. Singh, Phys. Rev. E **63**, 011206 (2001).
  - [32] S.-H. Chong, W. Götze, and M. R. Mayr, Phys. Rev. E **64**, 011503 (2001).
  - [33] S.-H. Chong and W. Götze, Phys. Rev. E **65**, 041503 (2002).
  - [34] S.-H. Chong and W. Götze, Phys. Rev. E **65**, 051201 (2002).
  - [35] T. Franosch, M. Fuchs, W. Götze, M. R. Mayr, and A. P. Singh, Phys. Rev. E **55**, 7153 (1997).
  - [36] M. Fuchs, J. Non-Cryst. Solids **172–174**, 241 (1994).
  - [37] A. Bondi, J. Phys. Chem. **68**, 441 (1964).
  - [38] J.-P. Hansen and I. R. McDonald, *Theory of Simple Liquids* (Academic Press, London, 1986), 2nd ed.
  - [39] B. Bernu, J.-P. Hansen, Y. Hiwatari, and G. Pastore, Phys. Rev. A **36**, 4891 (1987).
  - [40] J. N. Roux, J.-L. Barrat, and J.-P. Hansen, J. Phys.: Condens. Matter **1**, 7171 (1989).
  - [41] C. Bennemann, W. Paul, J. Baschnagel, and K. Binder, J. Phys.: Condens. Matter **11**, 2179 (1999).
  - [42] M. Fuchs, I. Hofacker, and A. Latz, Phys. Rev. A **45**, 898 (1992).
  - [43] W. Kob and H. C. Andersen, Phys. Rev. E **52**, 4134 (1995).
  - [44] J. Horbach and W. Kob, Phys. Rev. E **64**, 041503 (2001).
  - [45] F. Sciortino, L. Fabbian, S.-H. Chen, and P. Tartaglia, Phys. Rev. E **56**, 5397 (1997).
  - [46] W. Petry and J. Wuttke, Transp. Theory Stat. Phys. **24**, 1075 (1995).
  - [47] S. R. Kuchadkar and J. M. Wiest, J. Chem. Phys. **103**, 8566 (1995).
  - [48] S. Mossa, R. Di Leonardo, G. Ruocco and M. Sampoli, Phys. Rev. E **62**, 612 (2000); S. Mossa, G. Ruocco and M. Sampoli, Phys. Rev. E **64**, 021511 (2001).
  - [49] C. Theis and R. Schilling, Phys. Rev. E **60**, 740 (1999).
  - [50] S.-H. Chong and F. Hirata, J. Chem. Phys. **111**, 3083 (1999).
  - [51] T. Franosch and Th. Voigtmann, J. Stat. Phys. **109**, 237 (2002).
  - [52] W. Kob, M. Nauroth, and F. Sciortino, J. Non-Cryst. Solids **307–310**, 181 (2002).
  - [53] M. Aichele and J. Baschnagel, Eur. Phys. J. E **5**, 229 (2001); **5**, 245 (2001).
  - [54] B. Farago, A. Arbe, J. Colmenero, R. Faust, U. Buchenau, and D. Richter, Phys. Rev. E **65**, 051803 (2002).